




Magnetic ordering in $\text{La}_{1.5}\text{Ca}_{0.5}\text{CoO}_4$ revealed by resonant magnetic x-ray scattering and neutron diffraction

G. Subías ^{1,2,*}, J. Blasco ^{1,2,†}, J. Herrero-Martín ³, J. A. Rodríguez-Velamazán,⁴
M. Valvidares,³ R. Fan,⁵ P. Steadman,⁵ and J. García^{1,2}

¹*Instituto de Nanociencia y Materiales de Aragón (INMA), CSIC-Universidad de Zaragoza, Zaragoza 50009, Spain*

²*Departamento de Física de la Materia Condensada, Universidad de Zaragoza, C/ Pedro Cerbuna 12, Zaragoza 50009, Spain*

³*ALBA Synchrotron Light Source, Carrer de la Lluna 2-26, 08290 Cerdanyola del Vallès, Barcelona, Spain*

⁴*Institut Laue-Langevin, 71 avenue des Martyrs, CS 20156, 38042 Grenoble Cedex 9, France*

⁵*Diamond Light Source, Didcot, Oxfordshire OX11 0DE, United Kingdom*



(Received 22 January 2021; revised 24 March 2021; accepted 5 May 2021; published 20 May 2021)

We report a comprehensive study on the magnetic ground state of $\text{La}_{1.5}\text{Ca}_{0.5}\text{CoO}_4$ combining single crystal neutron diffraction and resonant magnetic x-ray scattering at the $\text{Co}L_{2,3}$ edges. Three single-crystal samples obtained from the same boule were investigated exhibiting magnetic phase transitions from a high-temperature paramagnetic phase to an antiferromagnetic phase at $T_N \approx 52$ K. Single crystal neutron diffraction reveals that the crystal structure at room temperature shows an orthorhombic A -centered lattice but with a and b axes almost equal in length. The structural phase transition (charge-ordering-like) from the parent tetragonal cell takes place above 523 K into the space group $A2mm$ where two nonequivalent compressed and expanded CoO_6 octahedra are ordered showing a checkerboard pattern in the ab plane. The charge segregation between the nonequivalent Co sites is about 0.4(1) electrons. Resonant magnetic x-ray reflections indexed as $(1/4, 1/4, 0)_t$, $(1/4, 1/4, 1)_t$, and $(1/4, 1/4, 1/2)_t$ in the parent tetragonal cell were observed at low temperature at the $\text{Co}L_{2,3}$ -edge energy range. The resonant spectral shape, with a noticeable absence of any resonant enhancement at the $\text{Co}L_2$ edge, indicates that only Co^{2+} -like ions participate in the magnetic ordering. The polarization analysis discloses that the orientation of Co magnetic moments is the same for the three magnetic orders and they are long-range ordered along the diagonal in the ab plane of the parent tetragonal cell with a slight tilt in the c axis. Despite the onset temperatures for the three resonant magnetic reflections being the same, ≈ 55 K, different thermal behavior is observed between $(1/4, 1/4, 1/2)_t$ and $(1/4, 1/4, L)_t$ ($L = \text{integer}$) reflections whose intensities maximize at different temperatures, suggesting the coexistence of two magnetic arrangements. Moreover, the intensity of the $(1/4, 1/4, 1/2)_t$ magnetic reflection is at least ten times larger than that of the $(1/4, 1/4, L)_t$ ($L = \text{integer}$) ones. On the other hand, neutron diffraction measurements only detect a single type of antiferromagnetic ordering following the propagation vector $\mathbf{k} = (1/4, 1/4, 1/2)_t$ that involves half of the Co atoms in the unit cell. We conclude that the bulk magnetic order in $\text{La}_{1.5}\text{Ca}_{0.5}\text{CoO}_4$ corresponds then to this propagation vector $\mathbf{k} = (1/4, 1/4, 1/2)_t$ while $(1/4, 1/4, 0)_t$ and $(1/4, 1/4, 1)_t$ magnetic reflections correspond to a minority magnetic phase that must be due to changes in the oxygen stoichiometry near the surface.

DOI: [10.1103/PhysRevB.103.184422](https://doi.org/10.1103/PhysRevB.103.184422)

I. INTRODUCTION

Hole-doped single-layered transition-metal perovskites have attracted the attention of many researchers due to their intriguing and diverse properties [1–3]. These compounds adopt the K_2NiF_4 tetragonal cell ($I4/mmm$) at high temperature. Initially it was thought that universal properties had been detected in half doped single-layered perovskites [4]. In this way, $\text{La}_{0.5}\text{Sr}_{1.5}\text{MnO}_4$ and $\text{La}_{1.5}\text{Sr}_{0.5}\text{CoO}_4$ are characterized by a checkerboard charge order (CO) at relatively high temperature that is followed by magnetic orderings at much lower temperature [5–7]. However, significant differences began to be revealed between different families of these

compounds. Starting from CO, in $\text{La}_{1-x}\text{Sr}_{1+x}\text{MnO}_4$ samples, the checkerboard CO is stable on cooling but the actual charge disproportionation is very small [8] and it is only commensurate for $x = 0.5$. Overdoped samples exhibit incommensurate reflections that can be explained on the basis of a charge density wave whose periodicity is related to the number of Mn $3d$ holes [9]. On the other hand, in $\text{La}_{2-x}\text{Ca}_x\text{CoO}_4$ the checkerboard CO remains commensurate for doping values well away from the optimal value of $x = 0.5$. [10,11] The reason for the difference between the $\text{La}_{1-x}\text{Sr}_{1+x}\text{MnO}_4$ and the $\text{La}_{2-x}\text{Ca}_x\text{CoO}_4$ series is their different chemical behavior. While layered manganites keep their nominal oxygen stoichiometry and Sr doping induces holes in the Mn $3d$ orbitals, $\text{Co}^{+2.5}$ mixed valence is very stable in layered cobaltates and Ca(Sr) doping rather produces changes in the oxygen stoichiometry of the samples (interstitial oxygen excess for underdoped samples and vacancies for overdoped ones) [12]. The CO state is thus very robust and the checkerboard pattern

*Corresponding author: gloria@unizar.es

†Corresponding author: jbc@unizar.es

gets composed of expanded and compressed CoO_6 octahedra with a charge disproportionation between the two Co sites of about 0.4(1) electrons, [11] that is, approximately half the expected value between nominal Co^{2+} and Co^{3+} .

Focusing on the magnetic properties, the differences can be even greater given the ability of Co atoms to appear under different spin states in the case of cobaltates. Co^{2+} is one of the few electronic configurations in 3d metals where the orbital angular moment acquires a significant non-negligible value. Moreover, Co^{3+} can adopt up to three different electronic configurations: low spin Co^{3+} (LS, $t_{2g}^6 e_g^0$), intermediate spin Co^{3+} (IS, $t_{2g}^5 e_g^1$), and high spin Co^{3+} (HS, $t_{2g}^4 e_g^2$). Preliminary magnetic studies on single crystals of $\text{La}_{1.5}\text{Sr}_{0.5}\text{CoO}_4$ revealed a strong anisotropic behavior with significantly higher magnetic susceptibility values when the magnetic field is parallel to the tetragonal ab plane (χ_{ab}) than when it is parallel to the c axis [13]. A broad maximum in the $\chi_{ab}(T)$ curve at about 60 K is indicative of the onset of magnetic correlations. The authors concluded the occurrence of HS- Co^{3+} ions but they did not contemplate the unquenched orbital moment of Co^{2+} . A later study using soft x-ray absorption spectroscopy at the Co $L_{2,3}$ edges disclosed that Co^{3+} are LS for $\text{La}_{1.5}\text{Sr}_{0.5}\text{CoO}_4$ in agreement with a full multiplet analysis [14,15]. Moreover, our recent study on the Co K_β emission spectra of $\text{La}_{1.5}\text{Sr}_{0.5}\text{CoO}_4$ and $\text{La}_{1.5}\text{Ca}_{0.5}\text{CoO}_4$ confirms that HS- Co^{2+} is the only magnetic atom in these compounds [12]. Neutron scattering measurements found that although magnetic correlations start at 60 K, the long-range magnetic order is only achieved below 31 K. Above that temperature, the existence of a spin canting or the loss of coherence between magnetic domains [16] is suggested. The magnetic structure is characterized by a slightly incommensurate vector, $\mathbf{k} = (1/4 - \delta, 1/4 - \delta, 0)_t$ with $\delta = 0.005$, in the frame of the tetragonal $I4/mmm$ cell (indicated by the subscript t). The magnetic order only affects half of the Co ions in the cell (HS- Co^{2+}), and the magnetic peaks are broad indicating a small coherence length and competitive magnetic interactions. Moreover, the magnetic properties seem to be very sensitive to small variations of the samples. In this way, a recent work on a polycrystalline $\text{La}_{1.5}\text{Sr}_{0.5}\text{CoO}_4$ sample reported a Griffiths-like phase at high temperature indicating that short CO correlation lengths seem to favor glassiness. The authors proposed a metamagnetic transition at low temperature and a stabilization of the antiferromagnetic (AFM) state at a magnetic field of 2.2 kOe [17].

Although $\text{La}_{1.5}\text{Ca}_{0.5}\text{CoO}_4$ is isostructural to $\text{La}_{1.5}\text{Sr}_{0.5}\text{CoO}_4$, the CO correlation length of the Ca-based system is longer than that of the Sr-based one [11,18]. Accordingly, the AFM phase is more stable and long range magnetic ordering appears at about 55 K [10]. Neutron scattering measurements revealed two types of magnetic reflections. Sharp magnetic reflections follow the propagation vector $\mathbf{k}_1 = (1/4, 1/4, 1/2)_t$ while broad reflections follow the propagation vector $\mathbf{k}_2 = (1/4, 1/4, 0)_t$ [18]. The presence of these two magnetic reflections in $\text{La}_{1.5}\text{Ca}_{0.5}\text{CoO}_4$ recalls previous studies on the $\text{La}_{0.5}\text{Sr}_{1.5}\text{MnO}_4$ manganite. In this sample, CO is made up of two magnetic atoms (nominally Mn^{3+} and Mn^{4+}) and the two magnetic propagation vectors agree with a CE-type magnetic structure [19], consisting of

ferromagnetic zigzag chains in the ab plane that are coupled antiferromagnetically with each other and along the c axis. This similarity led Horigane *et al.* [18] to suggest that Co^{3+} would not be in a LS state in $\text{La}_{1.5}\text{Ca}_{0.5}\text{CoO}_4$. A later work by the same authors extended the study to the $\text{La}_{2-x}\text{Ca}_x\text{CoO}_4$ ($0.3 \leq x \leq 0.8$) series [10]. In the lower doping region ($x < 0.5$), only magnetic peaks with the propagation vector $\mathbf{k}_1 = (1/4, 1/4, 1/2)_t$ are observed while in the high doping region ($x > 0.5$), the magnetic periodicity agrees with the propagation vector $\mathbf{k}_2 = (1/4, 1/4, 0)_t$. Half doping seems to be a critical point where both types of magnetic reflections coexist. This result weakens the hypothesis of a magnetic Co^{3+} to stabilize a CE-type magnetic structure. Nevertheless, the authors reported in the same study [10] a different set of weak magnetic reflections following the propagation vector $\mathbf{k}_3 = (1/8, 0, 1/2)_t$ originating from HS- Co^{3+} but a definitive magnetic structure has not been proposed. All this mixture of magnetic components makes $\text{La}_{1.5}\text{Ca}_{0.5}\text{CoO}_4$ a unique compound very interesting to study where it is possible to learn about the correlation between the spin configuration and magnetic interactions. With this purpose, we have performed a thorough study on the magnetic order of $\text{La}_{1.5}\text{Ca}_{0.5}\text{CoO}_4$ using single crystal neutron diffraction and resonant magnetic x-ray scattering (RMXS) at the Co $L_{2,3}$ edges on the same specimens. Full polarization analysis [20] of selected RMXS reflections is performed to determine the precise magnetic structure. Despite using the same single crystals for the two experiments the obtained results seem to be contradictory. Whereas $(1/4, 1/4, 1/2)_t$, $(1/4, 1/4, 0)_t$, and $(1/4, 1/4, 1)_t$ magnetic reflections were observed by RMXS, only $(1/4, 1/4, 1/2)_t$ -type reflections were detected in single crystal neutron diffraction. This controversy is explained as due to the enhanced sensitivity of RMXS in the soft x-ray region to the sample surface and hence to small changes in the oxygen stoichiometry near the surface.

II. EXPERIMENT

Polycrystalline $\text{La}_{1.5}\text{Ca}_{0.5}\text{CoO}_4$ was prepared by the solid state chemistry method as reported elsewhere [11]. The powders were pressed into rods and sintered at 1300 °C to be used for crystal growth. This growth was carried out in a homemade floating zone furnace [21] with two semielliptical mirrors, in dry air atmosphere with a growth speed of 6 mm/h. The total length of the obtained crystalline rod was 55 mm with a diameter of 4 mm. Single crystals with a typical cylindrical shape (diameter of 4 mm and length of 3 mm) were cut from the boule with different orientations. The chemical composition of the boules was tested using wavelength dispersive x-ray fluorescence spectrometry (Advant'XP+ model from Thermo-ARL) and the La:Ca:Co stoichiometry agreed with the expected values within the experimental error (1%). Selected parts of the boule were ground and previously characterized by synchrotron x-ray powder diffraction [12]. Rietveld analysis of the x-ray patterns using the FULLPROF package program [22] indicated that the crystal was a single phase without detectable impurities [23]. The oxygen content of $\text{La}_{1.5}\text{Ca}_{0.5}\text{CoO}_{4.02}$ was determined by cerimetric titration and an automatic Crison titrator. The studied single crystal

displays an oxygen stoichiometry/nominal average Co oxidation state of $\text{La}_{1.5}\text{Ca}_{0.5}\text{CoO}_{4.02}/\text{Co}^{2.54+}$ [12].

Magnetic measurements were carried out between 2 and 300 K by using a commercial superconducting quantum interference device (SQUID) magnetometer from Quantum Design. The measurements were performed warming the sample after zero-field cooling (ZFC) and field cooling (FC) conditions at two different external magnetic fields (0.1 and 50 kOe).

Neutron diffraction experiments on two single crystals were performed at two four-circle instruments of the Institute Laue Langevin (Grenoble, France). D9 was used to determine the crystal structure at room temperature. A single crystal with cylindrical-like shape was glued with the $[1, 1, 0]_t$ direction in the horizontal plane and a wavelength of $\lambda = 0.834 \text{ \AA}$ was used. D10 was employed to determine the magnetic contribution. Two crystals of the same boule, the one characterized at D9 and a second crystal with a polished $[1, 1, 4]_t$ direction, were measured yielding similar results. A helium-flow cryostat was utilized to vary temperatures between 2 and 60 K and a $\lambda = 2.36 \text{ \AA}$ was used to be more sensitive to the low Q region.

Three single crystals of the same growth were cut and polished to achieve mirrorlike surfaces normal to the $[1, 1, 0]_t$, $[1, 1, 2]_t$, and $[1, 1, 4]_t$ directions in order to respectively investigate the presence of $(1/4, 1/4, 0)_t$, $(1/4, 1/4, 1)_t$, and $(1/4, 1/4, 1/2)_t$ magnetic reflections using soft x rays. RMXS was carried out at the $\text{Co } L_{2,3}$ absorption edges using two beamlines from two synchrotron facilities: BOREAS-BL29 beamline [24] of ALBA (Cerdanyola del Vallès, Spain) and I10 beamline of the Diamond Light Source (Didcot, UK). The energy dependence of all magnetic reflections was recorded at the MaRes end station of the BOREAS beamline. The crystal $\text{La}_{1.5}\text{Ca}_{0.5}\text{CoO}_{4.02}$ $(110)_t$ was mounted on the diffractometer with the $[0, 0, 1]_t$ crystal axis perpendicular to the beam propagation direction in grazing incidence ($\theta = 0^\circ$). In this experimental configuration, the electric-field vector of the incident beam was adjusted parallel (linear σ polarization) or normal (linear π polarization) to the c axis which is orthogonal to the scattering plane [Fig. 1(a)]. A helium-flow cryostat allows sample cooling down to 20 K in ultrahigh vacuum conditions. The BOREAS undulator allows changing the polarization of the incident beam in a continuous way from σ to π but no polarization analyzer for the scattered beam is provided. This is not the case for Diamond's I10 beamline, where two W/B4C multilayer polarization analyzers optimized for working at the $\text{Co } L_{2,3}$ absorption edge energies [Fig. 1(b)] allowed a full polarization analysis of the scattered beam [25]. We note here that the same sample crystals were used in the experiments at the two synchrotron beam lines. The 2θ angles found for $(1/4, 1/4, 0)_t$, $(1/4, 1/4, 1)_t$, and $(1/4, 1/4, 1/2)_t$ at the $\text{Co } L_{2,3}$ edges (770–800 eV) were within $91\text{--}96^\circ$, $143\text{--}160^\circ$, and $103\text{--}109^\circ$ ranges, respectively. On the other hand, $\text{Co } L_{2,3}$ -edge polarization-dependent x-ray absorption spectroscopy (XAS) spectra of the crystal $\text{La}_{1.5}\text{Ca}_{0.5}\text{CoO}_{4.02}(1, 1, 0)_t$ were measured in total-electron-yield (TEY) mode with incident light polarization $\varepsilon \parallel c$ ($\varepsilon \perp c$) at the HECTOR XMCD end station of the BOREAS beamline at room temperature under no applied magnetic field.

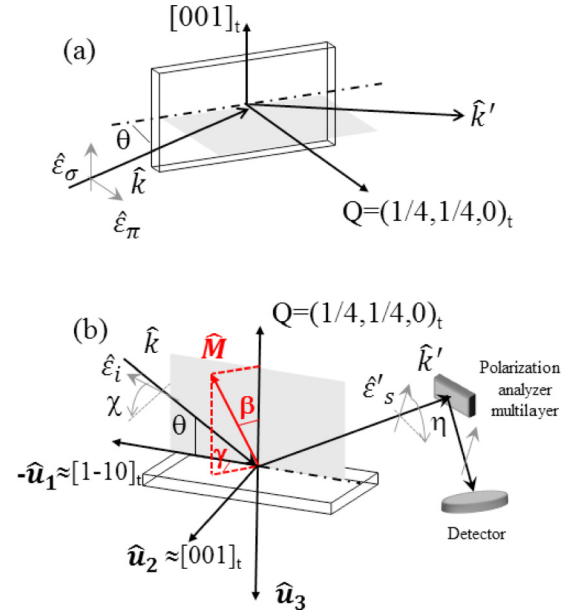


FIG. 1. (a) Experimental configuration of the BOREAS magnetic scattering end station at ALBA operating in a horizontal scattering geometry. The incident x-ray polarization $\hat{\varepsilon}_\sigma$ is perpendicular to the scattering plane and $\hat{\varepsilon}_\pi$ is parallel to the scattering plane. (b) Experimental configuration of the I10 magnetic scattering end station at Diamond operating in a vertical scattering geometry. The incident ($\hat{\varepsilon}_i$) and scattered ($\hat{\varepsilon}'_s$) x-ray polarization vectors are defined by χ and η , respectively and the \hat{u}_i vectors define a basis for the magnetic structure. $\chi(\eta) = 0^\circ$ and $\chi(\eta) = 90^\circ$ correspond to an incident (scattered) beam with σ and π polarization, respectively. In both scattering reference frames, \hat{k} and \hat{k}' are the incident and scattered wave vectors and 2θ is the scattering angle of the magnetic reflection.

III. RESULTS

The experiments were performed on a specimen previously characterized by synchrotron x-ray powder diffraction [12]. The pattern at room temperature agrees with a tetragonal lattice (space group $I4/mmm$) without significant splitting of diffraction peaks (Supplemental Material Fig. S1 [23]). However, the presence of a superstructure peak at temperatures up to 523 K that vanishes at 623 K [23] reveals that the cell is no longer tetragonal (see inset of Fig. S1). This is consistent with a previous report [26] that revealed a tiny orthorhombic distortion compatible with the space group $A2mm$ using the convergent-beam electron diffraction technique. $A2mm$ is a subgroup of $I4/mmm$ with the following transformation matrix of their lattice parameters: $a_o = (1, 1, 0)_t$, $b_o = (-1, 1, 0)_t$ and $c_o = (0, 0, 1)_t$. This tetragonal to orthorhombic structural transition is related to the CO differentiating two Co ions with different charge [10–12,26]. This type of transition was also reported for $\text{La}_{1.5}\text{Sr}_{0.5}\text{CoO}_4$ despite no clear transition being determined but the CO state persisted at least up to 600 K [7,27].

Magnetic properties were also measured in our single crystal [23] (see Fig. S2). Magnetic anisotropy is observed between the measurements carried out with the external field parallel or perpendicular to the c axis. In both cases, the

temperature dependence of the magnetic susceptibility shows a peak at 69 K indicating the onset of a magnetic phase transition typical of an AFM ordering. These properties agree with the ones reported for similar crystals [13,26].

A. Resonant magnetic x-ray scattering

Figure 2 compares Co $L_{2,3}$ XAS spectra and the energy dependence of the RMXS intensity at $(1/4, 1/4, 0)_t$, $(1/4, 1/4, 1/2)_t$, and $(1/4, 1/4, 1)_t$ reflections across the Co $L_{2,3}$ edge at 20 K, below T_N . The linearly polarized XAS spectra [Fig. 2(a)] show similar spectral features to those observed [14] in the Co $2p$ XAS spectra of $\text{La}_{1.5}\text{Sr}_{0.5}\text{CoO}_4$. The spectra are dominated by the Co $2p$ core-hole spin-orbit coupling which splits the spectrum roughly in two parts, namely, the L_3 ($E \approx 776\text{--}784$ eV) and L_2 ($E \approx 793\text{--}797$ eV) white line regions. As for the RMXS spectra, we observe the occurrence of strong resonances at the Co L_3 edge but no resonant features can be roughly seen at the Co L_2 edge that resembles very much the resonant spectral line shape of Co^{2+} -based oxides [28]. In addition, RMXS spectra of the three studied magnetic reflections show the same spectral features [Fig. 2(b)–2(d)]. We have compared the energy dependent RMXS spectra with a simulation obtained by $|f_m'|^2 + |f_m''|^2$, taking into account that the imaginary part of the magnetic scattering amplitude (f_m'') is proportional to the x-ray magnetic circular dichroism (XMCD) data [29] and the real f_m' and imaginary f_m'' parts are related to each other by a Kramers-Kronig transformation (inset of Fig. 3). Figure 3 compares the measured RMXS spectrum at $\mathbf{Q} = (1/4, 1/4, 1/2)_t$, corrected from self-absorption effects by multiplying it by the average XAS line shape, with the spectrum simulated using the experimental XMCD data of a polycrystalline $\text{La}_{1.5}\text{Sr}_{0.5}\text{CoO}_{4.02}$ sample measured at 300 K at an applied magnetic field of 6 T as f_m'' . The simulated RMXS spectrum reproduces the experimental one quite well suggesting that both RMXS and XMCD signals should originate from the same Co electronic and magnetic state. Furthermore, the XMCD is also almost zero at the Co L_2 edge while it is largely negative at the L_3 edge (inset of Fig. 3). This is a direct indication that the orbital contribution to the Co magnetic moment must be important [30]. The unquenched orbital moment in Co oxides has been closely related to the high-spin $\text{Co}^{2+} 3d^7$ electronic configuration [28,30]. Therefore, the three resonant reflections are originated by the same Co electronic structure that is the high-spin Co^{2+} .

The temperature evolution of the integrated intensity of the three resonant reflections at the maximum of the Co L_3 edge (778.5 eV) is displayed in Fig. 4. All three reflections disappear above ~ 55 K, consistent with the onset of the antiferromagnetic ordering deduced from the magnetic susceptibility data (see the Supplemental Material [23]). This points to a magnetic origin of these resonant reflections. However, we observe a clearly different thermal behavior between the magnetic ordering with $\mathbf{Q} = (1/4, 1/4, 1/2)_t$ and those with $\mathbf{Q} = (1/4, 1/4, L)_t$ with L integer. The magnetic resonant contribution for $(1/4, 1/4, 1/2)_t$ strongly increases below 55 K and maximizes at $T \approx 40$ K. On the other hand, the intensity for both $(1/4, 1/4, 1)_t$ and $(1/4, 1/4, 0)_t$ reflections show a smoother increase, saturating at a lower temperature of 30 K. We note here that all reflections were

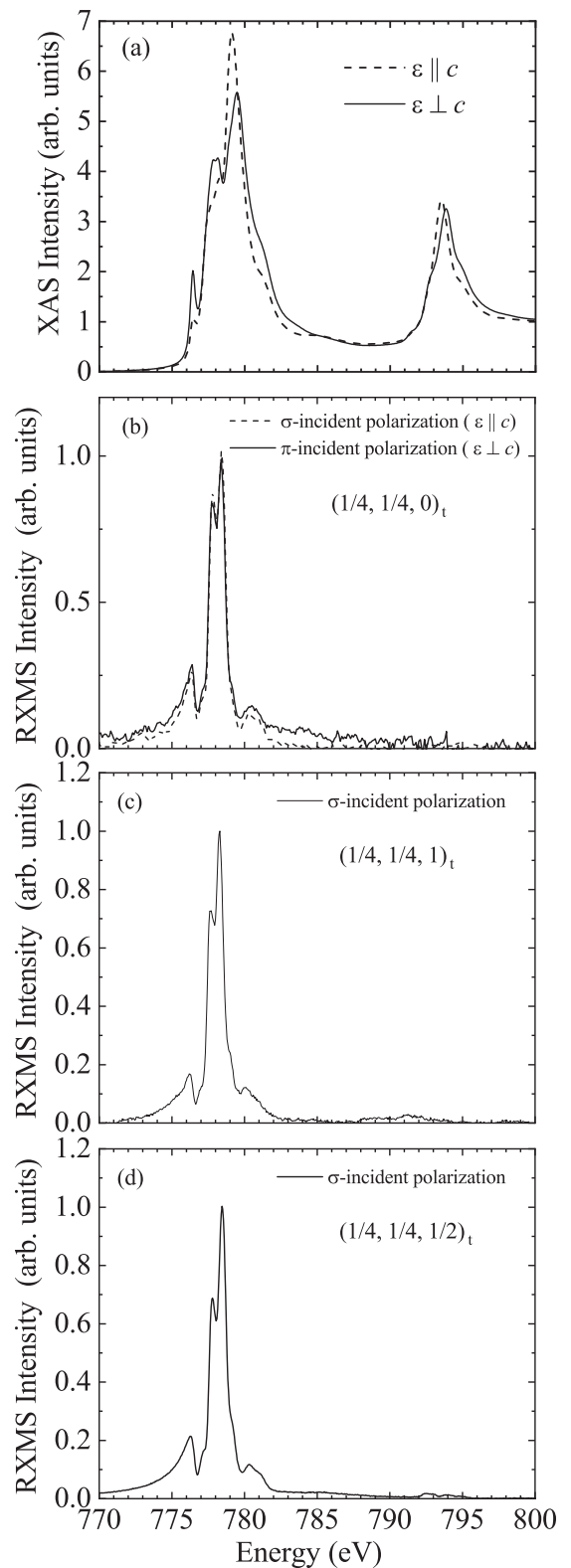


FIG. 2. Total-electron-yield Co $L_{2,3}$ edges x-ray absorption spectra measured at room temperature (a) and energy dependence of the $(1/4, 1/4, 0)_t$ magnetic reflection intensity at 20 K across Co $L_{2,3}$ edges of $\text{La}_{1.5}\text{Ca}_{0.5}\text{CoO}_{4.02}$ $(1, 1, 0)$ single crystal for σ (broken lines) and π (solid lines) incident x-ray polarizations (b). Energy dependence of the $(1/4, 1/4, 1/2)_t$ (c) and $(1/4, 1/4, 1)_t$ (d) magnetic reflection intensities at 20 K across Co $L_{2,3}$ edges for σ incident x-ray polarization.

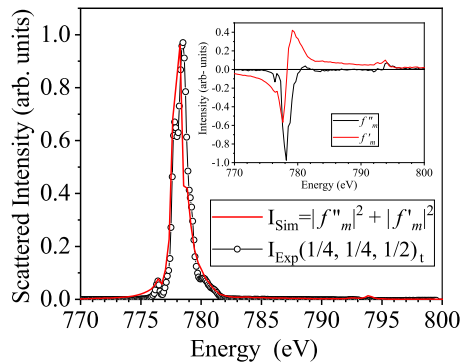


FIG. 3. Co $L_{2,3}$ energy scan of the RMXS intensity in $\text{La}_{1.5}\text{Ca}_{0.5}\text{CoO}_{4.02}$ at $\mathbf{Q} = (1/4, 1/4, 1/2)_t$ after correction for self-absorption effects compared to a simulated RMXS spectrum obtained from the measured XMCD signal. The inset shows the real and imaginary parts of the magnetic scattering at the Co $L_{2,3}$ edges in $\text{La}_{1.5}\text{Ca}_{0.5}\text{CoO}_{4.02}$.

normalized to their value at base temperature in Fig. 4 but the $(1/4, 1/4, 1/2)_t$ reflection shows about ten times larger intensity than the other two analyzed reflections, namely $(1/4, 1/4, 0)_t$ and $(1/4, 1/4, 1)_t$. Therefore, we can conclude that two different magnetic ordered phases are present in $\text{La}_{1.5}\text{Ca}_{0.5}\text{CoO}_{4.02}$, even if both can be associated to the same high-spin Co^{2+} electronic ground state.

The amplitude of a RMXS signal depends anisotropically on the direction of the magnetic moments. Thus, we performed a polarization analysis of the three resonant reflections to first unambiguously prove their magnetic character and second determine the orientation of the Co^{2+} magnetic moment. In the case of Co $L_{2,3}$ electronic dipole transition, the resonant scattering form factor for a single magnetic ion at site j is to first order given by

$$f_j(E) = f_0 \cdot (\hat{\epsilon}'_s \cdot \hat{\epsilon}_i) - if_1(\hat{\epsilon}'_s \times \hat{\epsilon}_i) \cdot \hat{m}_j, \quad (1)$$

where $\hat{\epsilon}_i$ and $\hat{\epsilon}'_s$ are the polarization unit vectors of the incident and scattered x rays, respectively; the f_0 and f_1 terms are the

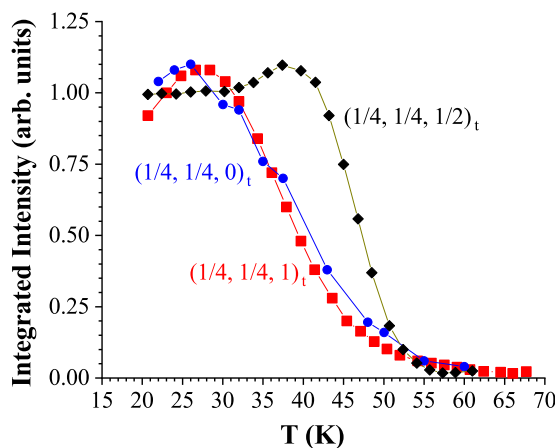


FIG. 4. Temperature dependence of integrated intensities of magnetic reflections with $q = (1/4, 1/4, 0)_t$ (blue circles), $q = (1/4, 1/4, 1)_t$ (red squares), and $q = (1/4, 1/4, 1/2)_t$ (black diamonds) at the maximum of Co L_3 edge. All reflections were normalized to their value at base temperature (~ 20 K) for comparison.

charge and linear magnetic part of the energy-dependent resonant amplitude, respectively, and \hat{m}_j is the unit magnetization vector at the j th site. The f_0 term describes the anomalous charge scattering and the f_1 term accounts for the resonant magnetic scattering ($f_m + if'_m$). Although f_0 and f_1 terms are energy dependent, we can take them as constant since the x-ray energy is fixed during the polarization analysis. Therefore, the structure factor for a resonant magnetic reflection becomes just a function of the momentum transfer, given by the scattering vector $\mathbf{Q} = \mathbf{k}' - \mathbf{k}$, where $\mathbf{k}(\mathbf{k}')$ is the wave vector of the incident (scattered) x rays,

$$F(\mathbf{Q}) \propto \sum_j f_j \exp(i\mathbf{Q} \cdot \mathbf{r}_j), \quad (2)$$

where the summation is over the Co sites with position vector \mathbf{r}_j .

For a collinear antiferromagnetic order, all the Co magnetic moments are parallel to a unique axis and the polarization dependence of the magnetic scattering is the same as for a single Co site in Eq. (1). Furthermore, as it will be mentioned later, the scattered intensity for the three measured reflections in the $\sigma - \sigma'$ polarization channel is zero so the anomalous charge scattering amplitude is strictly zero and the structure factor gets reduced to

$$F(\mathbf{Q}) \propto -iF_1(\hat{\epsilon}'_s \times \hat{\epsilon}_i) \cdot \hat{M} \quad (3)$$

with $F_1 = \sum_j \exp(i\mathbf{Q} \cdot \mathbf{r}_j) \cdot f_1$ and \hat{M} the unit magnetization vector. Thus, the dependence of the scattered intensities (proportional to F^2) on the incident and scattered polarization vectors and the Co magnetic moment direction can be easily modelled.

The general orthogonal coordinates frame ($\hat{u}_1, \hat{u}_2, \hat{u}_3$) used in resonant magnetic x-ray scattering [31–33] has been considered for our polarization analysis [Fig. 1(b)]. The components of \hat{M} are defined in standard spherical coordinates by the polar (β) and the azimuth (γ) angles with respect to the direction of the scattering vector \mathbf{Q} and a direction $-\hat{u}_1$ in the perpendicular plane [Fig. 1(b)]. The incident ($\hat{\epsilon}_i$) and scattered ($\hat{\epsilon}'_s$) x-ray polarization vectors are defined by χ and η angles, respectively. We have then fitted the experimental polarization analysis curves for the three magnetic reflections at the Co L_3 edge using Eq. (3) for the structure factor with β and γ angles as the only fitting parameters.

Figure 5 shows the experimental scattered intensities at the maximum of the Co L_3 edge (778.5 eV) for the $(1/4, 1/4, 0)_t$ reflection as a function of the incident x-ray polarization vector defined in the scattering frame by the χ angle [Fig. 1(b)]. The experimental dependence follows a sinusoidal behavior with $\chi = 0^\circ$ and $\chi = 90^\circ$ corresponding to an incident beam with σ and π polarization, respectively. The total scattered intensity is almost independent of the incident x-ray polarization χ for the $(1/4, 1/4, 0)_t$ reflection [Fig. 5(a)], which is a clear indication that the Co magnetic moment should lie almost along the scattering vector. In this crystal, the scattering plane contains the $-\hat{u}_3 = [1, 1, 0]_t$ and $-\hat{u}_1 = [1, -1, 0]_t$ crystallographic directions whereas the $\hat{u}_2 = [0, 0, 1]_t$ crystallographic direction is perpendicular to the scattering plane [Fig. 1(b)]. In this experimental configuration, the polar (β) and the azimuth (γ) angles are defined with respect to the $[1, 1, 0]_t$ and the

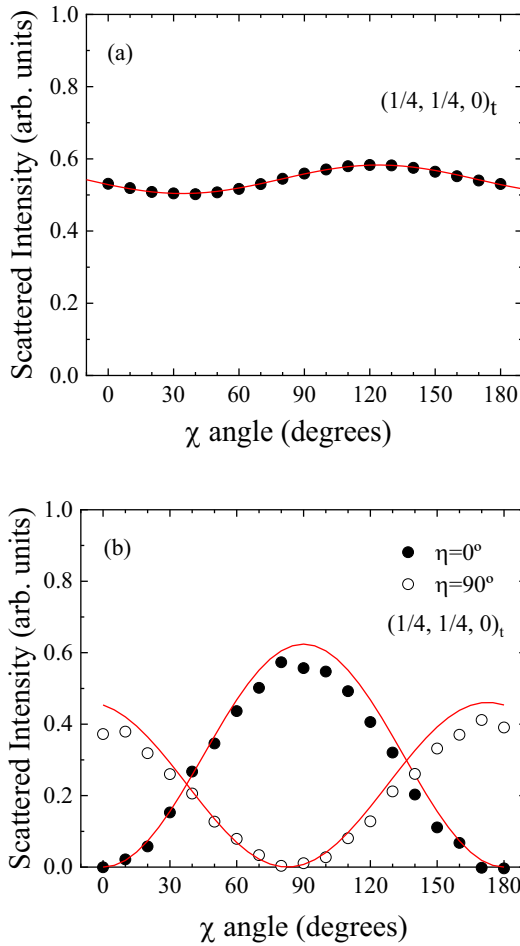


FIG. 5. Full polarization analysis of the $(1/4, 1/4, 0)_t$ magnetic reflection at 20 K. In top panel (a), total scattering intensity is recorded at the maximum of the $\text{Co } L_3$ edge as a function of the incident x-ray polarization χ . Circles denote the experimental data whereas red lines are the best fitted curves. Alternatively, in bottom panel (b), the $\text{Co } L_3$ edge scattered intensity is plotted as a function of χ for two different η positions of the multilayer analyzer.

$[1, -1, 0]_t$ crystallographic directions, respectively. The best fit for the orientation of the magnetic moment in this crystal yielded $\beta = 3(1)^\circ$ and $\gamma = 75(5)^\circ$. Values in parentheses are estimated errors in the last digit. This indicates that the direction of the Co magnetic moment is along the $[110]_t$ crystallographic direction, i.e., along the diagonal in the tetragonal ab plane, with a likely slight tilt towards the c -axis direction [Fig. 1(b)]. We note here that the $\text{La}_{1.5}\text{Ca}_{0.5}\text{CoO}_{4.02}$ crystal is twinned in the ab plane so the two domains with $\mathbf{Q} = [1, 1, 0]_t$ and $\mathbf{Q} = [1, -1, 0]_t$ are indistinguishable.

To verify the accuracy of these results, we have also measured the scattered intensity as a function of the incident x-ray polarization χ for different orientations η of the multilayer analyzer that serves as an x-ray polarizer [Fig. 1(b)]. Figure 5(b) shows the experimental polarization analysis curves of the $(1/4, 1/4, 0)_t$ reflection for two different positions η of the multilayer analyzer compared to the best fits obtained. $\chi = \eta = 0^\circ$ corresponds to the so-called $\sigma - \sigma'$ scattering channel that leads to systematic extinction according

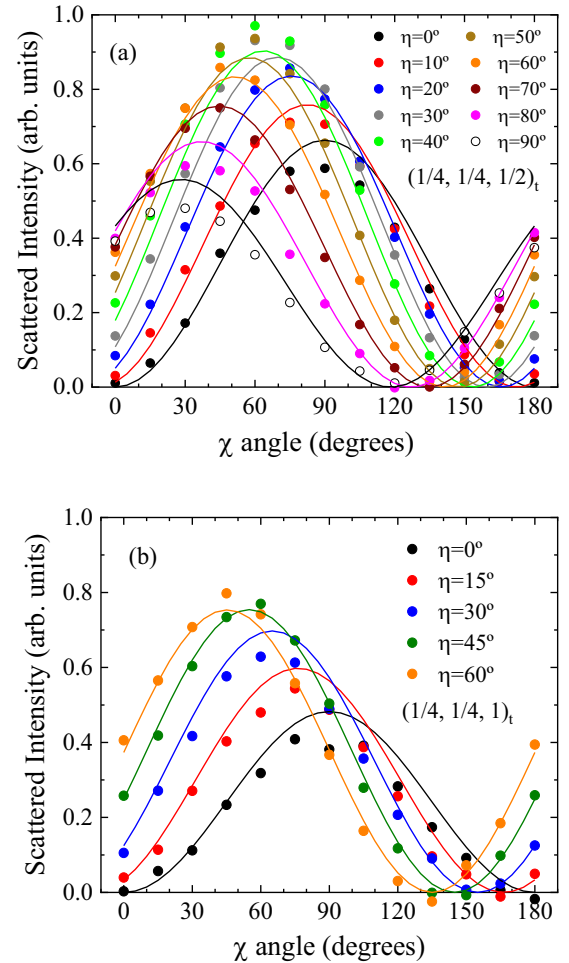


FIG. 6. Full polarization analysis of $(1/4, 1/4, 1/2)_t$ (a) and $(1/4, 1/4, 1)_t$ (b) magnetic reflections at 20 K. The $\text{Co } L_3$ edge scattered intensity is plotted as a function of χ for different η positions of the multilayer analyzer. Circles denote the experimental data whereas solid lines are the best fitted curves.

to the RMXS theory [31–33]. For the $(1/4, 1/4, 0)_t$ resonant reflection, the $\text{Co } L_3$ experimental scattered intensity in the $\sigma - \sigma'$ channel was zero, confirming that this reflection is of magnetic origin [Fig. 5(b)]. The orientation of the Co magnetic moments as obtained from the best fits corresponds to $\beta = 173(1)^\circ$ [or $-7(1)^\circ$] and $\gamma = -135(5)^\circ$ for $(1/4, 1/4, 0)_t$. Within the errors, these values agree with Co magnetic moments aligned along almost the same direction as that aforementioned using no polarization analyzer [Fig. 5(a)] but opposite in sign.

The experimental full polarization analysis curves of the $(1/4, 1/4, 1/2)_t$ and $(1/4, 1/4, 1)_t$ reflections are plotted in Fig. 6 as a function of the incident and scattered x-ray beam polarization vectors, denoted by χ and η , respectively. Best fit calculated curves are also shown in Fig. 6. Again, a sinusoidal behavior was found in both cases and the $\text{Co } L_3$ experimental scattered intensity in the $\sigma - \sigma'$ channel ($\chi = \eta = 0^\circ$) was zero, confirming that both $(1/4, 1/4, 1/2)_t$ and $(1/4, 1/4, 1)_t$ were also magnetic reflections. The best fit for the orientation of the Co magnetic moments yielded $\beta = 156.8(1)^\circ$ [or $-23.2(1)^\circ$] and $\gamma = -250(5)^\circ$

TABLE I. Fractional atomic coordinates and anisotropic temperature factors (\AA^2) of the $\text{La}_{1.5}\text{Ca}_{0.5}\text{CoO}_{4.02}$ single crystal obtained from Rietveld analysis of neutron diffraction data at room temperature. The x coordinate of Co1 was fixed as origin. The lattice parameters are $a = 5.4247(1)\text{\AA}$, $b = 5.4128(1)\text{\AA}$, and $c = 12.3702(2)\text{\AA}$. The reliability factors of the fit were $R_F = 0.029$ and $R_w = 0.039$.

	Co1	Co2	La/Ca1	La/Ca2	O1 _{basal}	O2 _{basal}	O3 _{apical}	O4 _{apical}
x	0	0.503(6)	0.003(5)	0.503(4)	0.242(5)	0.751(5)	0.000(5)	0.499(4)
y	0	0.5	0	0.5	0.2494(5)	0.7542(5)	0	0.5
z	0	0	0.36145(5)	0.36221(5)	0	0	0.16681(7)	0.17375(8)
B_{11}	0.004(2)	0.003(2)	0.0051(6)	0.0040(6)	0.002(2)	0.004(2)	0.0114(9)	0.0157(9)
B_{22}	0.0020(3)	0.0024(3)	0.0050(1)	0.00051(1)	0.0039(3)	0.0043(3)	0.0113(2)	0.0156(2)
B_{33}	0.0009(1)	0.0011(1)	0.0008(1)	0.0007(1)	0.0023(2)	0.0019(1)	0.0012(1)	0.0013(1)
B_{12}	0	0	0	0	-0.0015(7)	0.0005(6)	0	0
B_{13}	0	0	-0.0006(2)	-0.0006(2)	0	0	0.0012(4)	-0.0002(4)
B_{23}	0	0	0	0	0	0	0	0

for the $(1/4, 1/4, 1/2)_t$ reflection [Fig. 6(a)]. Meanwhile, $\beta = 136(1)^\circ$ [or $-44(1)^\circ$] and $\gamma = -272(5)^\circ$ were found for the $(1/4, 1/4, 1)_t$ reflection [Fig. 6(b)]. The dependence of the total scattered intensity of the $(1/4, 1/4, 1/2)_t$ and $(1/4, 1/4, 1)_t$ reflections upon the incident x-ray polarization χ was also measured for completeness (Fig. S3 [23]), giving consistent results with the aforementioned full polarization analysis [23].

For these two single crystals with $\mathbf{Q} = (1/4, 1/4, 1/2)_t$ and $\mathbf{Q} = (1/4, 1/4, 1)_t$, only the crystallographic direction of the scattering vector is known in the experimental configuration. Thus, only the refined polar (β) angles can give us information on the orientation of the magnetic moment within the crystallographic unit cell for the $(1/4, 1/4, 1/2)_t$ and $(1/4, 1/4, 1)_t$ magnetic reflections. We recall here that the polarization analysis of the $(1/4, 1/4, 0)_t$ reflection showed that the Co magnetic moments lie almost along the $[1, 1, 0]_t$ crystallographic direction. To check if the same orientation of the Co magnetic moments is found for the other two magnetic orders, we have calculated the angles formed between the $[1, 1, 0]_t$ and either the $[1, 1, 2]_t$ or the $[1, 1, 4]_t$ crystallographic planes. These angles are 23.7° and 41.3° , respectively and agree within the error with the polar β angles deduced from the best fits of the polarization analysis curves of the $(1/4, 1/4, 1/2)_t$ and $(1/4, 1/4, 1)_t$ magnetic reflections. Therefore, the orientation of the Co magnetic moments we derive is—within the errors—the same for the three magnetic orders, i.e., along a diagonal of the tetragonal ab plane slightly off-tilted along the c axis.

B. Neutron diffraction

The structure analysis at room temperature was performed using single crystal neutron diffraction since this technique is more sensitive to the position of oxygen atoms than x-ray diffraction. The crystal symmetry at 295 K is confirmed as orthorhombic with a and b axes almost equal in length. The observed reflections agreed with an A -centered lattice arising from the distortion of the high temperature cell with $a_0 \approx \sqrt{2}a_t$. The crystal is heavily twinned in the ab plane. The A -centering cell implies some extinction rules ($k + l = 2n + 1$ and the comparison of the reflections allowed by each domain indicates that the crystal seems to have a perfect twinning with an even ratio of the two domains. Following

previous studies [26], the experimental data were refined using the space group symmetry $A2mm$ (no. 35, standard setting $Cmm2$). The results yielded by the best fit are summarized in Table I. These results are similar to those published by Horigane *et al.* [26] but we observe a minor polar distortion in our sample. In fact, our experimental data can be fitted using the centrosymmetric space group $Ammm$ with similar accuracy. If we look at the errors derived for x coordinates (Table I), only one basal oxygen atom significantly shifts from the inversion center position. In the previous report [26], this happened with the apical oxygen atoms. We have applied a symmetry mode analysis using the AMPLIMODES program [34] to gain insights into the transition from the high temperature phase into the orthorhombic one. Table II shows the mode decomposition for this transition with a comparison of the normalized amplitudes between the two refinements. In both cases, the primary mode for the transition belongs to the irrep $X1+$ while modes belonging to the irreps $GM1+$ and $X4-$ are secondary. The main difference between both refinements concerns the value of the polar modes belonging to the irrep $GM5-$, which are larger for the data reported by Horigane *et al.* [26] although the estimated error in these modes is much higher than in the rest (around 36%). The global distortion calculated for this transition is small, 0.12 and 0.17 \AA for the data reported by this study and by Horigane *et al.* [26], respectively. That small distortion was consistent with the difficulty in detecting it using x-ray diffraction techniques [23].

Our refinement distinguishes two distinct Co environments that give rise to two types of CoO_6 octahedra. Co1O_6 is compressed with the following interatomic

TABLE II. Summary of mode decompositions of the $A2mm$ structure with respect to the parent $I4/mmm$ structure of $\text{La}_{1.5}\text{Ca}_{0.5}\text{CoO}_{4.02}$ reported in this work and in Ref. [26].

K vector	Irrep	Direction	Dim.	Amplitude (\AA)	
				This work	Horigane <i>et al.</i> [26]
(0,0,0)	GM1+	(a)	2	0.028	0.022
(0,0,0)	GM5-	(a, a)	5	0.055	0.105
(1/2,1/2,0)	X1+	$(a, -a)$	4	0.103	0.119
(1/2,1/2,0)	X4-	$(a, -a)$	3	0.013	0.049

distances: Co1-O1 = 1.883(19) Å, Co1-O2 = 1.896(19) Å, and Co1-O3 = 2.0635(9) Å. Co2O₆ is expanded with longer bond lengths: Co2-O1 = 1.961(30) Å, Co2-O2 = 1.924(29) Å, and Co2-O4 = 2.149(1) Å. The bond valence sum (BVS) method was used to estimate the charge disproportionation between the two nonequivalent Co sites. Using the reference parameters [35] for Co³⁺, BVS calculation yields oxidation state values of +2.65(5) and +2.25(7) for Co1 and Co2, respectively. However, using the reference parameters [36] for Co²⁺, the results are +3.05(5) and +2.61(7), respectively. Both calculations agree with a checkerboard pattern of compressed and expanded CoO₆ octahedra with a charge segregation of 0.44(7) electrons between the two Co sites, in agreement with previous reports [11,12]. If we average out the two calculations, we obtain +2.43(7) for Co2 and +2.87(5) for Co1 as oxidation states, in excellent agreement with our previous spectroscopic results [12].

Figure 7 shows different Q scans performed at 2 K in the single crystal with surface normal to the $[1, 1, 0]_t$ direction. Charge-superstructure reflections are shown in Fig. 7(a) in the Q scan along the $[1, 0, L]_O$ direction referred to the orthorhombic cell (indicated by the subscript O) as their intensity remains almost constant upon heating up to 55 K [Fig. 7(c)]. We note here that the tetragonal $(h/2, h/2, l)_t$ and $(h/2, -h/2, l)_t$ reflections transform into the orthorhombic $(h, 0, l)_O$ and $(0, k, l)_O$ ones, respectively. Due to the symmetry conditions of the $A2mm$ space group, the $(0, k, l)_O$ reflections are only allowed for $k + l = \text{even}$ while the $(h, 0, l)_O$ ones are allowed for $l = \text{even}$. We observe structural reflections for both $L = \text{even}$ and $L = \text{odd}$, as expected for a crystal with perfect twin structure. On the other hand, the magnetic contribution appeared in the neutron patterns below 55 K [Fig. 7(c)]. The new magnetic peaks follow the propagation vector $\mathbf{k}_1 = (1/2, 0, 1/2)_O$ as shown in Fig. 7(b). There is no indication of any other type of magnetic contribution as no $(1/2, 0, l)_O$ reflections with l integer were detected [Fig. 7(b)]. This result is at odds with a previous report [26] and our own results using the RMXS technique (see previous section). Therefore, we decided to mount the single crystal with a polished $(1, 1, 4)_t$ face where $(1/2, 0, l)_O$ with l integer magnetic peaks had been detected by RMXS. The results were identical to the previous crystal and we only detected the same family of $(h/2, 0, l/2)_O$ magnetic peaks.

In order to analyze the magnetic structure, the strong twinning should be taken into account since we detected both $(h/2, 0, l/2)_O$ and $(0, k/2, l/2)_O$ sets of magnetic peaks, each one coming from one of the two domains. Accordingly, it is hard to differentiate between the two possible $\mathbf{k}_1 = (1/2, 0, 1/2)_O$ or $\mathbf{k}'_1 = (0, 1/2, 1/2)_O$ propagation vectors in a crystal with a perfect twinning. In the case of \mathbf{k}_1 , the basic IRREPS of the $A2mm$ space group offer two possible solutions, either the moments of the magnetic atom (Co²⁺ like) are coupled antiferromagnetically along the orthorhombic b axis or they are within the ac plane. The refinements clearly opt for the second option with the moments mainly aligned along the a_0 axis with a small tilt in the c direction. It is noteworthy that as $A2mm$ is a noncentrosymmetric group, the propagation vector \mathbf{k}_1 is not equivalent to $-\mathbf{k}_1$ and the occurrence of two propagation vectors within the first Brill-

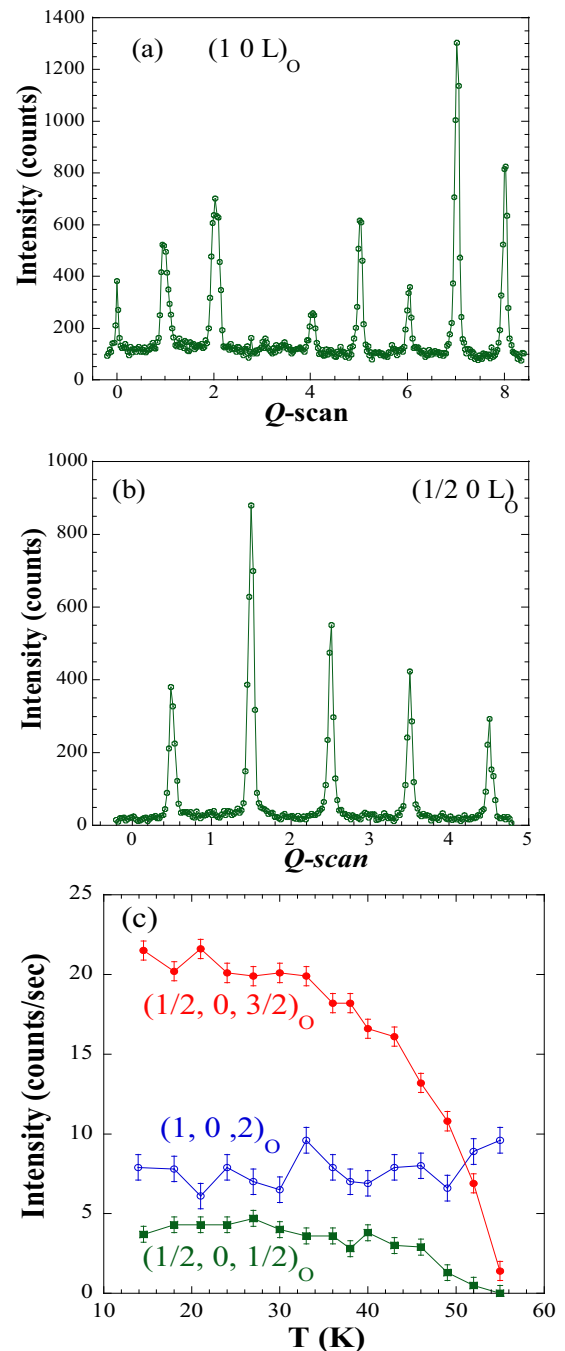


FIG. 7. Reciprocal space (Q) scans along the $[1, 0, L]_O$ (a) and $[1/2, 0, L]_O$ (b) directions at 2 K in La_{1.5}Ca_{0.5}CoO_{4.02} single crystal. (c) Temperature variation of intensities of structural $(1, 0, 2)_O$ and magnetic $(1/2, 0, 1/2)_O$ and $(1/2, 0, 3/2)_O$ reflections. For the sake of clarity, it is noteworthy to remember that $(1, 0, L)_O$ and $(1/2, 0, L)_O$ orthorhombic reflections are equivalent to $(1/2, 1/2, L)_t$ and $(1/4, 1/4, L)_t$ tetragonal ones.

loun zone makes it hard to differentiate phase shifts between both vectors by diffraction techniques. In our case, the magnetic cell is commensurate and we have considered the same magnetic moment for all the Co²⁺-like sites in the cell in agreement with the RMXS results. The magnetic cell can be seen in Fig. 8. Regarding the orthorhombic ab plane, the

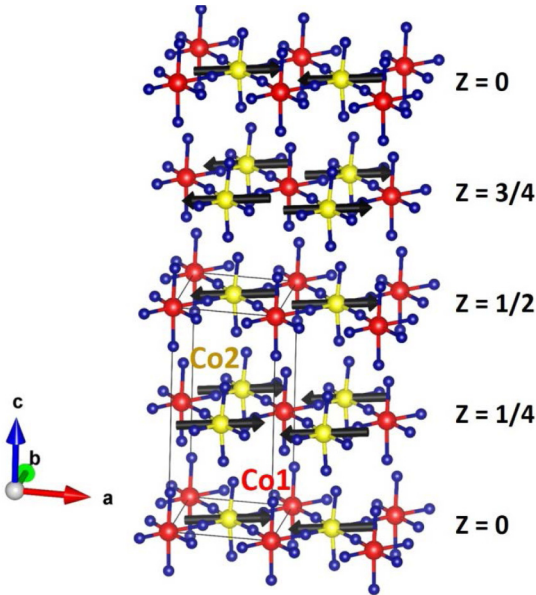


FIG. 8. Schematic view of the refined magnetic structure for the $\text{La}_{1.5}\text{Ca}_{0.5}\text{CoO}_{4.02}$ sample. For clarity, we only show Co atoms and basal oxygens.

magnetic ordering is the result of the AFM superexchange $\text{Co}^{2+}\text{-O-Co}^{3+}\text{-O-Co}^{2+}$ interaction (see later in the Discussion section). The magnetic structure shows an AFM alignment in one of the orthorhombic axes but FM in the other. Along the c axis, there is an AFM coupling between next-neighbor planes of CoO_6 octahedra, i.e., between Co^{2+} -like cations with $z = 0$ and $z = 1/2$ (or $z = 1/4$ and $z = 3/4$). Accordingly, any Co^{2+} -like moment displays an even mixture of FM and AFM couplings along this direction adopting a $\uparrow\uparrow\downarrow\downarrow$ structure (see Fig. 8). Finally, one must bear in mind that if the propagation vector were $\mathbf{k}'_1 = (0, 1/2, 1/2)_O$, the results would be orthogonal to those indicated in Fig. 8.

The ordered magnetic moment on the Co atom at 2 K in the antiferromagnetic phase is $\mu = 2.35(5)\mu_B$ with refined components $\mu_x = 2.35(5)$ and $\mu_z = 0.13(6)\mu_B$. This value is lower than the effective paramagnetic value obtained by the Curie-Weiss law in our recent x-ray absorption and emission spectroscopic study, which shows that its angular momentum is not completely quenched [12]. This study showed that the charge disproportionation in $\text{La}_{1.5}\text{Ca}_{0.5}\text{CoO}_{4.02}$ is not complete and Co^{2+} -like atoms in this compound are found to be in a mixed-valent state $\text{Co}^{2.4}$ with holes mainly located in Co $3d\text{-O}2p$ hybridized states. These covalent effects probably result in a reduced ordered magnetic moment. It is interesting to underline that similar values of ordered magnetic moments have been obtained from neutron diffraction for related high-spin Co^{2+} double-perovskites that are always lower than the corresponding effective paramagnetic moments [37].

IV. DISCUSSION AND CONCLUSIONS

We first discuss the disparity of results obtained by neutron diffraction experiments between the work of Horigane *et al.* [26] and the present study. In a second step, we comment on the inputs provided by our study using the combination

of two different but complementary techniques in the same single crystals.

Horigane *et al.* [26] reported on the occurrence of magnetic reflections in a $\text{La}_{1.5}\text{Ca}_{0.5}\text{CoO}_4$ crystal following two different propagation vectors: $(1/2, 0, 1/2)_O$ and $(1/2, 0, 0)_O$. These two types of magnetic peaks were only observed in a single specimen because underdoped samples (Ca content less than $x = 0.5$) only show magnetic peaks ascribed to the $\mathbf{k}_1 = (1/2, 0, 1/2)_O$ vector whereas overdoped compounds ($x > 0.5$) only display magnetism associated to the $\mathbf{k}_2 = (1/2, 0, 0)_O$ vector. In addition, similar changes are observed when the Co sublattice is slightly doped. Thus, doping with Cr stabilizes one type of magnetic reflections, $(h/2, k, l/2)_O$, while doping with either Mn or Fe gives place to only $(h/2, k, l)_O$ magnetic reflections [38]. The uniqueness of the $\text{La}_{1.5}\text{Ca}_{0.5}\text{CoO}_4$ specimen suggested that it was located at a critical point in the phase diagram where various types of magnetic arrangements are able to coexist. Furthermore, they reported on a third type of $(h/4, k/4, l/2)_O$ magnetic reflections suggesting that Co^{3+} should be also magnetic. Nevertheless, our present neutron diffraction measurements on two $\text{La}_{1.5}\text{Ca}_{0.5}\text{CoO}_{4.02}$ single crystals only detected one type of magnetic contribution ascribed to either $\mathbf{k}_1 = (1/2, 0, 1/2)_O$ or $\mathbf{k}'_1 = (0, 1/2, 1/2)_O$ propagation vectors.

On the other hand, RMXS experiments could successfully detect $(1/2, 0, 1/2)_O$, $(1/2, 0, 0)_O$, and $(1/2, 0, 1)_O$ magnetic peaks suggesting the occurrence of two magnetic phases, one of them hidden to neutron diffraction. In addition, the spectral shape of the RMXS spectra clearly concurs with the contributions of only HS Co^{2+} cation without any trace of the participation of Co^{3+} cations in the magnetic order for any of the two magnetic phases. Our previous spectroscopic study on the Co electronic (valence and spin) state of the $\text{La}_{2-x}\text{Ca}_x\text{CoO}_4$ series disclosed that the electronic state of Co is very similar for all $0.3 \leq x \leq 0.7$ compounds [12]. Co is in a fluctuating mixed valence state in the high temperature phase and below the CO transition, a partial charge disproportionation [$\delta \approx 0.5(1)$] leads to a checkerboard pattern of two distinct Co atoms. Therefore, we can conclude that the magnetic structure change between under- and overdoped samples cannot be ascribed to changes of the Co electronic state. Instead, we have observed the key role of the oxygen sublattice to modulate the charge ordering along this series, in agreement with the results previously reported for the Sr half-doped compound, where a significant hole density in the O $2p$ states was concluded [14]. Oxygen excess as interstitial oxygen around the La/Ca atoms is observed in underdoped samples while oxygen vacancies at the apical position are noticed in overdoped samples. Our $\text{La}_{1.5}\text{Ca}_{0.5}\text{CoO}_{4.02}$ crystal has a small oxygen excess so a ground magnetic state similar to that found in underdoped samples with $\mathbf{k}_1 = (1/2, 0, 1/2)_O$ propagation vector is a consistent result. On the other side, vacancies are usually formed on the oxide's surface. In such a case, sharp surface regions with oxygen vacancies can be magnetically ordered following the $\mathbf{k}_2 = (1/2, 0, 0)_O$ propagation vector as it happens in overdoped samples. The RMXS technique is very sensitive to surface properties (including magnetism) but it does also prove the magnetic order of the bulk crystal. Neutron diffraction, instead, is only sensitive

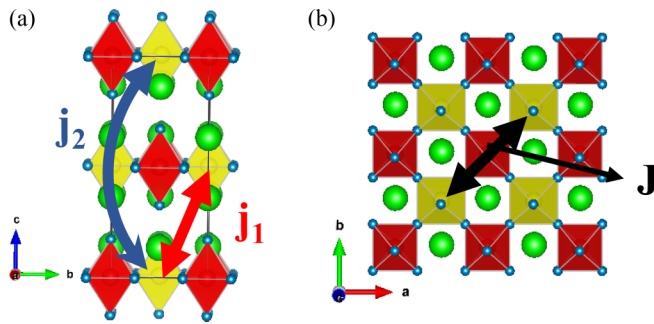


FIG. 9. (a) Projection of the orthorhombic crystal structure onto the bc plane and magnetic interactions along the z direction between Co2 in neighbor planes (j_1) and between Co2 in next-neighbor planes (j_2). (b) Projection onto the ab plane showing the straight magnetic interaction between Co2 cations through a Co1O₆ octahedron (J).

to the bulk magnetic structure and it would need a strong oxygen inhomogeneity along the whole specimen to detect the two types of magnetic orders by this technique. We recall here that the magnetic reflections correspondent to the $\mathbf{k}_2 = (1/2, 0, 0)_O$ propagation vector, although detected by RMXS, are an order of magnitude less intense than that of the bulk magnetic order, that is they correspond to a minority phase.

Regarding the different magnetic structures, their stability can be understood based on three AFM superexchange interactions (see Fig. 9). J is the in-plane superexchange interaction between Co²⁺-like cations through a nonmagnetic Co atom [Fig. 9(b)]. This is the strongest magnetic interaction in this structure and responsible for the large 2D coherence length in the magnetic arrangement. Along with this interaction, we hypothesize the existence of two other weaker magnetic interactions. One of them would occur between Co²⁺ cations located in neighboring rows along the c axis but shifted in the ab plane [j_1 in Fig. 9(a)]. The other interaction would connect, in a straight line parallel to the c axis, two Co²⁺ cations in the next-neighbor row along the c axis [j_2 in Fig. 9(a)]. We postulate that the disorder produced by interstitial oxygen atoms weakens j_1 and then $j_2 > j_1$. In this case, the magnetic structure follows the propagation vector $\mathbf{k}_1 = (1/2, 0, 1/2)_O$ [or $\mathbf{k}'_1 = (0, 1/2, 1/2)_O$]. However, the lack of interstitial oxygens firms up j_1 giving rise to an AFM ordering between neighboring planes along the z direction and in that case, the propagation vector is $\mathbf{k}_2 = (1/2, 0, 0)_O$ [or $\mathbf{k}'_2 = (0, 1/2, 0)_O$].

We have already mentioned that due to the strong twinning, the propagation vector for the main magnetic phase cannot be discriminated (\mathbf{k}_1 or \mathbf{k}'_1). Otherwise, this is not the case

for the minority phase that is only observed in the RMXS measurements. The simultaneous occurrence of $(1/2, 0, L)_O$ magnetic reflections with L even and odd can only be explained by a magnetic structure (see Fig. S4 [23]) following the propagation vector \mathbf{k}'_1 which implies the duplication of the orthorhombic b axis with the magnetic moments along this direction [23].

Summarizing, we have studied the structural and magnetic properties of a La_{1.5}Ca_{0.5}CoO_{4.02} single crystal using a combination of neutron diffraction and RMXS techniques. Our compound shows a nominal mixed valence of Co^{+2.54}, i.e., a bit overdoped but due to a slight excess of oxygen content, as deduced from x-ray absorption and emission spectroscopy [12]. We have identified the room temperature structure as an orthorhombic cell composed by a checkerboard arrangement of compressed and expanded CoO₆ octahedra in the ab plane. However, our work cannot unambiguously confirm the occurrence of a noncentrosymmetric structure. We have found that the magnetic ground state strongly depends on the oxygen content of the La_{2-x}Ca_xCoO_{4±δ} compounds in such a way that samples with an oxygen excess (as interstitial oxygen) exhibit a magnetic structure with double a (or b) and c axes with respect to the crystallographic orthorhombic cell. However, La_{2-x}Ca_xCoO_{4±δ} samples without the disorder produced by the presence of interstitial oxygen adopt a magnetic structure where only the b axis gets doubled. The latter magnetic structure is also found near the surface likely due to the presence of oxygen vacancies as a minority phase. Finally, in both magnetic structures, only the Co²⁺-like cations are magnetic (HS Co²⁺) and the magnetic moments are aligned along one of the orthorhombic a (or b) axes with a small tilt ($\approx 3^\circ$) in the z direction.

ACKNOWLEDGMENTS

These experiments were performed at BOREAS beamline at ALBA synchrotron with the collaboration of ALBA staff and we also acknowledge Diamond Light Source for beam time on instrument I10 under Proposal No. SI19996. We would also like to thank ILL for granting beam time (Experiment No. 5-41-1021). The authors would like to acknowledge the use of Servicio General de Apoyo a la Investigación - SAI, Universidad de Zaragoza. For financial support, we thank the Spanish Ministerio de Ciencia, Innovación y Universidades (Project No. RTI2018-098537-B-C22 co-funded by ERDF from EU) and Diputación General de Aragón (Project No. E12-20R).

[1] M. Imada, A. Fujimori, and Y. Tokura, *Rev. Mod. Phys.* **70**, 1039 (1998).
 [2] Y. Drees, D. Lamago, A. Piovano, and A. C. Komarek, *Nat. Commun.* **4**, 2449 (2013).
 [3] T. P. Croft, C. Lester, M. S. Senn, A. Bombardi, and S. M. Hayden, *Phys. Rev. B* **89**, 224513 (2014).

[4] I. A. Zaliznyak, J. M. Tranquada, G. Gu, R. W. Erwin, and Y. Moritomo, *J. Appl. Phys.* **95**, 7369 (2004).
 [5] B. J. Sternlieb, J. P. Hill, U. C. Wildgruber, G. M. Luke, B. Nachumi, Y. Moritomo, and Y. Tokura, *Phys. Rev. Lett.* **76**, 2169 (1996).
 [6] Y. Murakami, H. Kawada, H. Kawata, M. Tanaka, T. Arima, Y. Moritomo, and Y. Tokura, *Phys. Rev. Lett.* **80**, 1932 (1998).

- [7] I. A. Zaliznyak, J. M. Tranquada, R. Erwin, and Y. Moritomo, *Phys. Rev. B* **64**, 195117 (2001).
- [8] J. Herrero-Martín, J. Blasco, J. García, G. Subías, and C. Mazzoli, *Phys. Rev. B* **83**, 184101 (2011).
- [9] J. García, J. Herrero-Martín, G. Subías, J. Blasco, J. S. Andreu, and M. Concepción Sánchez, *Phys. Rev. Lett.* **109**, 107202 (2012).
- [10] K. Horigane, H. Hiraka, T. Uchida, K. Yamada, and J. Akimitsu, *J. Phys. Soc. Jpn.* **76**, 114715 (2007).
- [11] J. García, G. Subías, J. Blasco, M. C. Sánchez, and G. Beutier, *Phys. Rev. B* **97**, 085111 (2018).
- [12] G. Subías, J. Blasco, S. Lafuerza, V. Cuartero, M. C. Sánchez, R. Boada, S. Díaz-Moreno, F. Fauth, and J. García, *Inorg. Chem.* **59**, 15757 (2020).
- [13] Y. Moritomo, K. Higashi, K. Matsuda, and A. Nakamura, *Phys. Rev. B* **55**, R14725 (1997).
- [14] C. F. Chang, Z. Hu, H. Wu, T. Burnus, N. Hollmann, M. Benomar, T. Lorenz, A. Tanaka, H.-J. Lin, H. H. Hsieh, C. T. Chen, and L. H. Tjeng, *Phys. Rev. Lett.* **102**, 116401 (2009).
- [15] N. Hollman, M. W. Haverkort, M. Cwik, M. Benomar, M. Reuther, A. Tanaka, and T. Lorenz, *New J. Phys.* **10**, 023018 (2008).
- [16] L. M. Helme, A. T. Boothroyd, R. Coldea, D. Prabhakaran, C. D. Frost, D. A. Keen, L. P. Regnault, P. G. Freeman, M. Enderle, and J. Kulda, *Phys. Rev. B* **80**, 134414 (2009).
- [17] A. Ahad, D. K. Shukla, F. Rahman, K. Gautam, K. Dey, S. S. Majid, S. K. Sharma, and J. A. H. Coaquira, *Appl. Phys. Lett.* **113**, 102405 (2018).
- [18] K. Horigane, K. Yamada, H. Hiraka, and J. Akimitsu, *J. Magn. Mater.* **310**, 774 (2007).
- [19] S. Larochelle, A. Mehta, L. Lu, P. K. Mang, O. P. Vajk, N. Kaneko, J. W. Lynn, L. Zhou, and M. Greven, *Phys. Rev. B* **71**, 024435 (2005).
- [20] C. Mazzoli, S. B. Wilkins, S. Di Matteo, B. Detlefs, C. Detlefs, V. Scagnoli, L. Paolasini, and P. Ghigna, *Phys. Rev. B* **76**, 195118 (2007).
- [21] J. Blasco, M. C. Sánchez, J. García, J. Stankiewicz, and J. Herrero-Martín, *J. Cryst. Growth* **310**, 3247 (2008).
- [22] J. Rodríguez-Carvajal, *Phys. B (Amsterdam, Neth.)* **192**, 55 (1992), available at <https://www.ill.eu/sites/fullprof/>.
- [23] See Supplemental Material at <http://link.aps.org/supplemental/10.1103/PhysRevB.103.184422> for details about structural characterization of the polycrystalline $\text{La}_{1.5}\text{Ca}_{0.5}\text{CoO}_{4.02}$ sample by synchrotron x-ray powder diffraction, magnetic susceptibility data for the $\text{La}_{1.5}\text{Ca}_{0.5}\text{CoO}_{4.02}$ single crystal as a function of temperature and magnetic field, resonant magnetic x-ray scattering of $(1/4, 1/4, 1/2)_t$ and $(1/4, 1/4, 1)_t$ reflections without polarization analyzer, and the magnetic structure of the minority phase.
- [24] A. Barla, J. Nicolás, D. Cocco, S. M. Valvidares, J. Herrero-Martín, P. Gargiani, J. Moldes, C. Ruget, E. Pellegrin, and S. Ferrer, *J. Synchrotron Radiat.* **23**, 1507 (2016).
- [25] T. A. W. Beale, T. P. A. Hase, T. Iida, K. Endo, P. Steadman, A. R. Marshall, S. S. Dhesi, G. van der Laan, and P. D. Hatton, *Rev. Sci. Instrum.* **81**, 073904 (2010).
- [26] K. Horigane, H. Nakao, Y. Kousaka, T. Murata, Y. Noda, Y. Murakami, and J. Akimitsu, *J. Phys. Soc. Jpn.* **77**, 044601 (2008).
- [27] I. A. Zaliznyak, J. P. Hill, J. M. Tranquada, R. Erwin, and Y. Moritomo, *Phys. Rev. Lett.* **85**, 4353 (2000).
- [28] J. Herrero-Martín, A. N. Dobrynin, C. Mazzoli, P. Steadman, P. Bencok, R. Fan, A. A. Mukhin, V. Skumryev, and J. L. García-Muñoz, *Phys. Rev. B* **91**, 220403(R) (2015).
- [29] S. W. Lovesey and S. P. Collins, *X-Ray Scattering and Absorption by Magnetic Materials*, Oxford Series on Synchrotron Radiation (Clarendon, Oxford, 1996).
- [30] T. Burnus, Z. Hu, H. H. Hsieh, V. L. J. Joly, P. A. Joy, M. W. Haverkort, Hua Wu, A. Tanaka, H.-J. Lin, C. T. Chen, and L. H. Tjeng, *Phys. Rev. B* **77**, 125124 (2008).
- [31] M. Blume and D. Gibbs, *Phys. Rev. B* **37**, 1779 (1988).
- [32] J. P. Hill and D. F. McMorrow, *Acta Crystallogr., Sect. A* **52**, 236 (1996).
- [33] C. Detlefs, M. Sánchez del Rio, and C. Mazzoli, *Eur. Phys. J.: Special Topics* **208**, 359 (2012).
- [34] J. M. Pérez-Mato, D. Orobengoa, and M. I. Aroyo, *Acta Crystallogr., Sect. A* **66**, 558 (2010).
- [35] R. M. Wood and G. J. Palenik, *Inorg. Chem.* **37**, 4149 (1998).
- [36] I. D. Brown and D. Altermatt, *Acta Crystallogr., Sect. B* **41**, 244 (1985).
- [37] M. C. Viola, M. J. Martínez-Lope, J. A. Alonso, J. L. Martínez, J. M. De Paoli, S. Pagola, J. C. Pedregosa, M. T. Fernández-Díaz, and R. E. Carbonio, *Chem. Mater.* **15**, 1655 (2003).
- [38] K Horigane, H Hiraka, K Tomiyasu, K Ohoyama, D Louca, and K Yamada, *J. Phys.: Conf. Ser.* **340**, 012061 (2012).